Journal of Raman Spectroscopy

WILEY

Journal of RAMAN SPECTROSCOPY

RESEARCH ARTICLE OPEN ACCESS

Raman Study of the Slobodka Ordinary Chondrite

M. Simopoulou[1] | I. Baziotis[1] | L. Ferrière[2,3] | J. Hu[4] | C. Sanchez-Valle[5] | P. N. Gamaletsos[6] | D. Palles[7] | J. Berndt[5] | C. Ma[4] | S. Klemme[5] | P. D. Asimow[4]

[1]Agricultural University of Athens, Laboratory of Mineralogy & Geology, Athens, Greece | [2]Natural History Museum Abu Dhabi, Saadiyat Island, Abu Dhabi, UAE | [3]Natural History Museum Vienna, Vienna, Austria | [4]Division of Geological and Planetary Sciences, California Institute of Technology, Pasadena, California, USA | [5]University of Münster, Inst. of Mineralogy, Münster, Germany | [6]School of Mineral Resources Engineering, Technical University of Crete, Chania, Greece | [7]Theoretical & Physical Chemistry Inst., National Hellenic Research Foundation, Athens, Greece

Correspondence: I. Baziotis (ibaziotis@aua.gr)

Received: 30 January 2025 | **Revised:** 1 April 2025 | **Accepted:** 26 April 2025

Funding: The authors received no specific funding for this work.

Keywords: high-pressure polymorphs | L-chondrite | ordinary chondrite | Raman spectroscopy | shock stage classification | Slobodka meteorite

ABSTRACT

We carried out a detailed study of the texture, mineralogy, and spectroscopic properties of the Slobodka ordinary chondrite meteorite. Previous descriptions differ on the classification of this meteorite, so we re-evaluated its petrologic type and shock stage. The observed texture and mineral chemistry are most consistent with the L4 chondrites. It records features of strong shock metamorphism mostly consistent with shock stage S4, including irregular and planar fractures, undulatory extinction, and mosaicism in olivine, pyroxene, and plagioclase. The distribution of shock damage was further evaluated at the mesoscale, revealing significant heterogeneity: regions of shock stage S4 are located near shock melt veins, a few selected areas indicate shock stage S3, and areas farther away from shock melt veins exhibit shock stage S2. The application of a range of in-situ analytical techniques, including Raman spectroscopy and electron back-scatter diffraction as well as microprobe, revealed the presence of five preserved high-pressure phases within the investigated sample of Slobodka, namely albitic jadeite, tuite, majorite, wadsleyite, and xieite. Together, these findings demonstrate that Slobodka preserves textural and mineralogical characteristics indicative of the highly energetic impact that likely fragmented the parent body of the L-chondrites.

1 | Introduction

Meteorite classification can be challenging, especially for historical falls, due to limited and sometimes contradictory information in the existing databases MetBull (www.lpi.usra.edu/meteor/) and MetBase (which was recently merged into Astromat, www.astromat.org/collections/meteorites; [1]). MetBull contains only a short entry without any supporting data for most meteorites that came to light before about 1990. In addition to provenance questions, changes in compositional and textural classification standards and analytical technologies for identifying meteorite classes, petrologic types, and shock stages have evolved over decades and have not been consistently applied retroactively to all historical falls (e.g., Mocs meteorite; see MetBull). One consequence is that attempts to make statistical comparisons among the populations of meteorite falls and finds may be biased.

Moreover, recent discoveries concerning shock-induced phases and the high temperature and high pressure (HP) conditions at which they form motivate re-evaluation of the pressure–temperature–time history corresponding to each shock stage. For example, the presence, texture, and chemistry of the newly described phase albitic jadeite may become an important calibrant (alongside other HP phases with known stability fields) once it is synthesized in the laboratory [2–4]. It has been shown that albitic jadeite can be a homogeneous (single-phase) super-silicic, highly-vacant clinopyroxene [2], with a favorable pressure window for formation near 11.5 GPa [5]. Unfortunately, up to now, synthesis and compression studies of albitic jadeite are totally missing. However, continued study of (true) jadeite and the variety of albitic jadeite occurrences in terrestrial settings and meteorites, distinguishing metamorphic and melt-grown cases, will ultimately improve the definition of the structural properties of the various end members of the vacancy-stabilized high-pressure clinopyroxene group (Ma et al., 2022; Baziotis et al., 2022, 2025). This may ultimately lead to construction of a reliable geo-barometer.

The reassessment of historical meteorite entries is crucial to ensure accuracy in contemporary research and databases, exemplified by the case of the Slobodka meteorite. The entire entry for Slobodka meteorite, reads "L4 (fall, 1818)", while it is also listed as an L4 in Astromat database. However, Slobodka was reclassified by Rochette et al. [6] on the basis of modern electron microprobe and magnetic data as an H4. This example highlights the challenges of maintaining consistency in meteorite classification, particularly when new analytical techniques and data become available. Therefore, the reclassification underscores the necessity of reassessing historical classifications to reflect current scientific understanding and technology. Moreover, there may be some confusion about this meteorite because of another meteorite named "Slobodka (of P. Partsch)" which is described as "L6 (find, 1838)." Hence, one goal of the current study is to report new petrographic, compositional, and spectroscopic data on archived specimens of the original Slobodka meteorite to ensure that the class, petrologic type, and shock stage are consistently and definitively assigned according to current usage.

Slobodka is undoubtedly a shocked meteorite, as revealed by the presence of obvious shock melt (now glassy) veins which are visible at the macroscopic scale. It is important to note, the terminology we used throughout the current manuscript is as follows: the rock is divided into two major areas, the shock melt veins and the host rock. The shock melt veins comprise the melt vein clasts and the melt vein groundmass, while the host rock is composed by the chondrules and the matrix. Therefore with the term "groundmass" we mean the shock melt vein material that is not identified as unmelted clasts of the host rock or anything else, whereas "matrix" is corresponds to the material outside the shock melt vein that is not part of a recognizable chondrule. And regarding the shock melt veins in Slobodka in particular, they are composed of a mixture of glass, clasts from the adjacent host rock (commonly recrystallized), and newly crystallized phases. We used a complementary range of analytical techniques—including optical microscopy, Raman spectroscopy (RS), field emission scanning electron microscopy (FE-SEM), field emission electron probe microanalyzer (FE-EPMA), and electron backscatter diffraction (EBSD)—to characterize the texture, chemistry, and structure of the phases in the matrix and within the shock melt vein. These data support a thorough evaluation of the petrologic type and shock stage classification of Slobodka. In addition, for the first time for this meteorite, we identified five high-pressure phases—albitic jadeite, tuite, majorite, xieite, and wadsleyite—within a shock melt vein, recording information about the pressure–temperature–time path experienced during shock metamorphism [7]. We collected a detailed Raman transect across a shock melt vein to investigate how the Raman spectral features (e.g., Raman shift and peak shape) of albitic jadeite vary across the vein (i.e., a proxy for differences in cooling rate). The results suggest variations in the crystallinity of albitic jadeite as a function of the pressure–temperature–time path during or after crystal growth.

2 | Materials and Analytical Methods

2.1 | Material

Two polished thin sections of Slobodka (NHMW-L4372 and NHMW-O2607; both prepared from the same specimen) were obtained from the Natural History Museum Vienna (Austria) collection. The principal reason for this study was to re-evaluate the class, petrologic type, and shock stage of this historical fall. This required analysis of matrix, chondrules, and shock melt vein textures, mineralogy, and mineral chemistry at scales from individual grains to whole sections.

2.2 | Analytical Methods

2.2.1 | Texture

For textural analysis, mosaic maps of both thin sections (NHMW-L4372 and NHMW-O2607) were created from a series of plane-polarized transmitted-light optical photomicrographs (Figure S1A). The shock features of the grains and chondrules (Figures 1, 2, S1B, and S2) in these optical photomicrographs were used for shock stage classification according to established schemes [8–10].

2.2.2 | Scanning Electron Microscopy and Electron Back-Scatter Diffraction

Field emission scanning electron microscopy (FE-SEM; Zeiss 1550VP at Caltech and JEOL-JSM IT500L at Hellenic Survey of Geology & Mineral Exploration, Athens, Greece) yielded back-scattered electron (BSE) images and preliminary compositions by energy-dispersive X-ray spectroscopy (Ultim Max Oxford EDS detector). Semi-quantitative mineral analyses were performed with 20 kV accelerating voltage, 1.5 nA beam current, 20 s acquisition time, and 20 mm working distance. Electron backscatter diffraction (EBSD; HKL system attached to Zeiss 1550VP SEM at Caltech) was used to identify the structure of the HP phases in the shock melt vein. Single crystal EBSD analyses were performed at 20 kV and 6 nA (focused beam) with a 70° tilted stage on uncoated sections in "variable pressure" mode (25 Pa of N2 gas in the chamber to reduce specimen charging). The EBSD indexing and phase matching analyses were conducted using the Channel 5 software package. The Caltech Zeiss SEM was also used to collect low-accelerating voltage (10 kV) and therefore high spatial resolution EDS spectra for small phases such as chromite inclusions in plagioclase.

2.2.3 | Electron Probe Micro-Analysis

Mineral chemistry was determined using a FE-EPMA (JEOL JXA 8530F) at the Natural History Museum Vienna (NHMW),

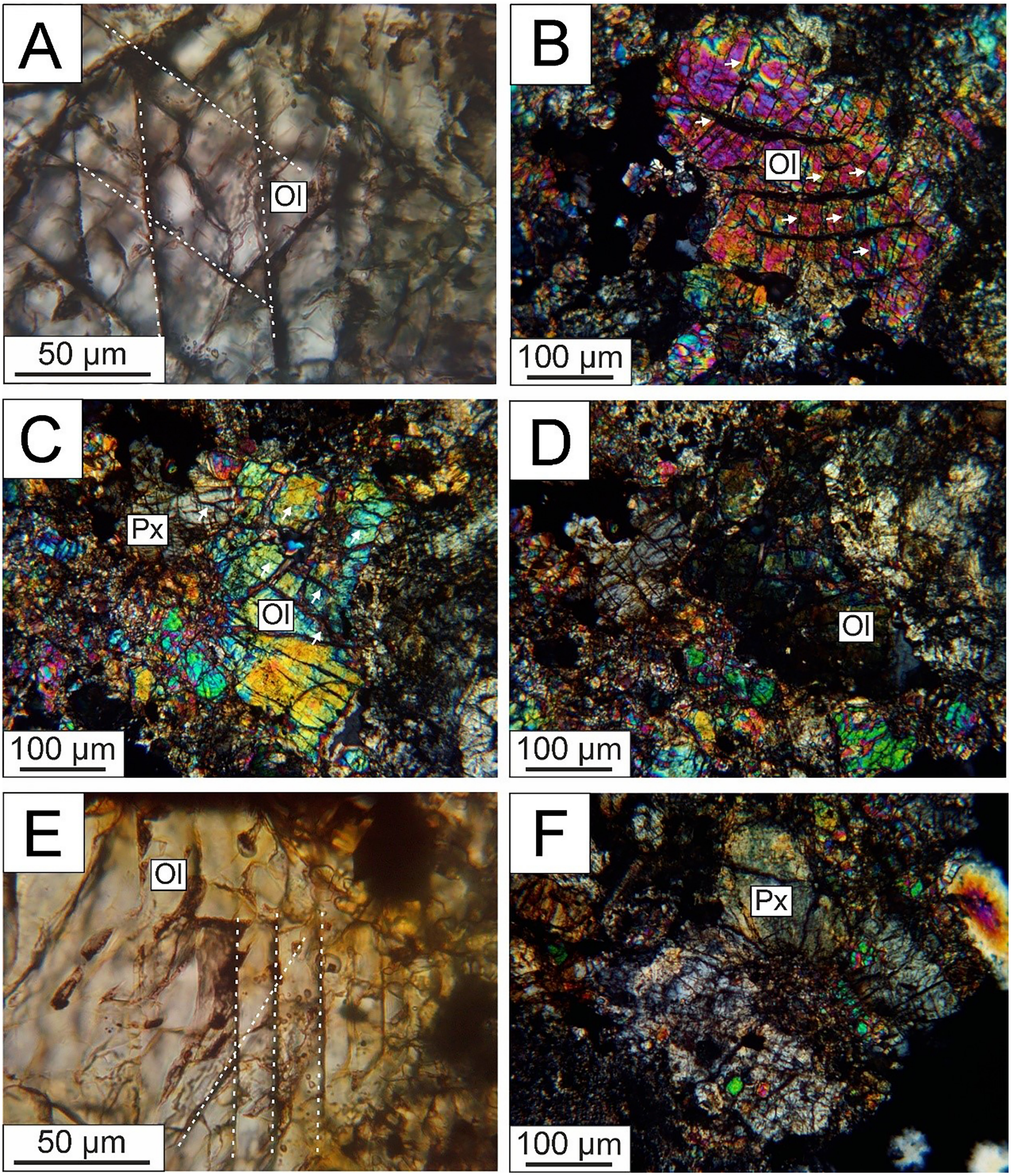

FIGURE 1 | (A) Two sets of planar fractures (few of them indicated by dashed white lines) in olivine (PPL). (B) Irregular fractures (some of them indicated by white arrows) in olivine (XPL). (C) Irregular fractures (some of them indicated by white arrows) in olivine and pyroxene (XPL). (D) undulatory extinction in olivine (XPL). (E) Two sets of planar fractures (few of them indicated by dashed white lines) in olivine (PPL). (F) Moderate to strong mosaicism in orthopyroxene (XPL). Ol, olivine; Px, pyroxene; PPL, plane-polarized light; XPL, cross-polarized light.

Austria, and at the Institut für Mineralogie, University of Münster, Germany, both equipped with five wavelength-dispersive spectrometers and one energy-dispersive spectrometer. Mineral analyses were performed with an accelerating voltage of 15 kV. For minerals, a 15 nA focused beam current, 20 s counting time on peak position, and 10 s for each background were used. For glass analyses, a slightly defocused (5 μm diameter) beam, 5 nA probe current, and counting times of 10 s on-peak and 5 s on each background position were used. Natural mineral standards used were albite (Na, Si, Al), wollastonite (Ca), olivine (Mg), almandine (Fe), spessartine (Mn), orthoclase (K), rutile (Ti), chromite (Cr), and Ni-oxide (Ni) with ZAF matrix correction.

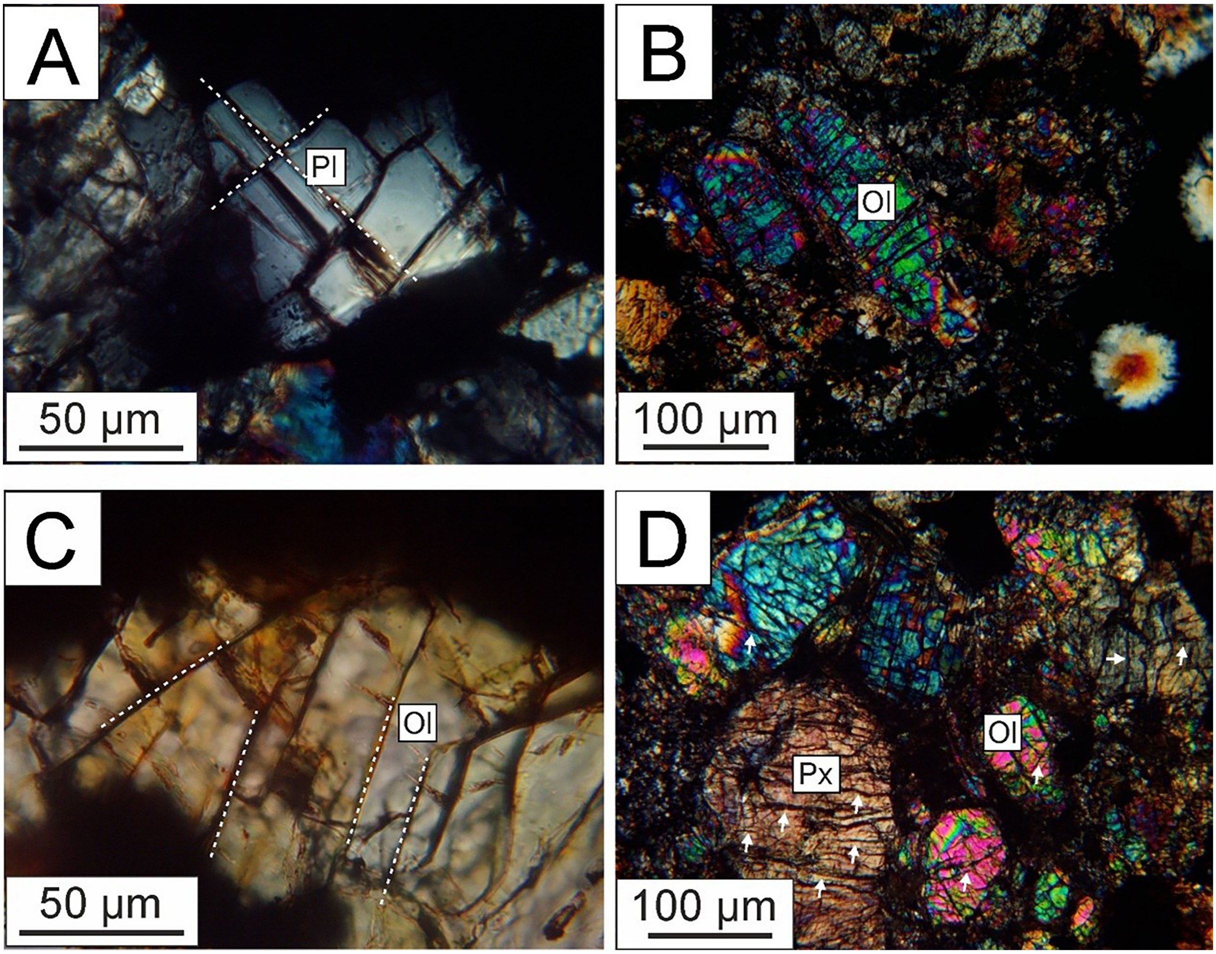

FIGURE 2 | (A) Plagioclase with irregular fractures (few of them indicated by dashed white lines) and undulatory extinction (XPL). (B) Planar fractures in olivine (XPL). (C) Two sets of planar fractures (few of them indicated by dashed white lines) in a relatively oxidized olivine crystal (PPL). (D) Irregular fractures (some of them indicated by white arrows) in olivine and pyroxene (XPL). Pl, plagioclase.

2.2.4 | Raman Spectroscopy

Raman Spectroscopy was used to identify the high-pressure phases within the shock melt vein. We used two Raman instruments: a Renishaw inVia Reflex at the Theoretical & Physical Chemistry Institute, National Hellenic Research Foundation (Athens, Greece) using a 514.5 nm wavelength laser and a 2400 line/mm diffraction grating; and a Horiba LabRam HR800 at the University of Münster (Germany) using a 632.8 nm excitation source and a 1800 line/mm grating. For both instruments, power was modulated to < 2 mW to minimize damage to the target. Each spectrum was collected using a 100× objective lens at a total acquisition time of 60 s averaging three accumulations, and spanning Raman shifts of 200–1200 cm^{-1}. We compared our Raman data for each HP mineral acquired with reference Raman spectra obtained from the RRUFF database (https://rruff.info).

2.2.5 | ImageJ/Fityk Software

The ImageJ/FIJI open-source image processing software was used for measuring the area of chondrules and calculating the modal abundance of chondrules and of metal in the two thin sections investigated. This software was also used to calculate the length of the shock melt vein and the relative distance of each analytical spot from the center of the shock melt vein. The Fityk software (version 0.9.8) was also used to fit a Lorentz–Gaussian peak shape for the evaluation of the full width at half maximum (FWHM) of the major peak at ~700 cm^{-1} of each individual Raman spectrum of albitic jadeite.

3 | Results

3.1 | Petrography and Mineral Chemistry of Matrix and Chondrules

Section NHMW-L4372 was examined at whole-section scale. It shows a light-colored interior cross-cut by a single dark vein. Some areas are stained orange, indicating oxidation of Fe-bearing minerals (Figure S1A). Eight areas in the matrix (including chondrules) were analyzed for their texture and mineral chemistry. The average chondrule size is in the range of ~0.7–1.1 mm and most chondrules can be easily distinguished from the surrounding matrix. Chondrule textures in Slobodka are mostly of radial pyroxene and barred olivine varieties, along with a few porphyritic chondrules; the low abundance of the latter likely reflects recrystallization and locally intense shock processes (Figure S2).

3.1.1 | Olivine

Olivine ($Fo_{75.2–76.6}$; based on 26 analyses) is the predominant mineral in the matrix (Table S1); crystal sizes vary from 100 µm to 1 mm. It exhibits various deformation-related features, including irregular fractures, up to two sets of planar fractures (Figures 1A,E and 2C), and undulatory extinction (Figure 1D).

3.1.2 | Pyroxene

Pyroxene shows both planar and irregular fractures (Figures 1C and 2D) and moderate mosaicism (Figure 1F). Most of the pyroxene analyses are classified (based on 26 analyses) as diopside to augite ($En_{46.8–54.9}Fs_{6.54–13}Wo_{32.1–46.4}$) or enstatite ($En_{76.0–78.9}Fs_{18.8–21.3}Wo_{1.2–4.6}$) (Table S2) in the En-Di-Hd-Fs quadrilateral [11].

3.1.3 | Plagioclase

Under transmitted light (crossed polars), the plagioclase in Slobodka is anisotropic; we have not identified any maskelynite in the studied thin sections. Undulatory extinction of plagioclase is common in proximity to the shock melt vein (Figure 2A). In addition, most of the plagioclase in the matrix and chondrules has irregular fractures. The plagioclase has a considerable range of compositions (based on 18 analyses), $Ab_{65.3–86.0}An_{9.26–25.2}Or_{4.54–10.0}$ (Table S3).

3.2 | Shock Melt Veins and Melt Pockets

3.2.1 | Characterization of High-Pressure Polymorphs Through Texture, Mineral Chemistry, and Raman Spectroscopy

We created BSE mosaic maps of the shock melt veins that occurred in both studied sections, NHMW-L4372 (Figure 3A) and NHMW-O2607 (Figure 3B). Each shock melt vein contains silicate grains, small and rounded blebs of Fe–Ni metal, oxides (chromite), and troilite as the main components. In NHMW-O2607, we also observed a melt-pocket containing glass with plagioclase composition and multiple clusters of chromite fragments (Figure S3). This melt-pocket borders a large orthopyroxene clast with µm-scale exsolution of clinopyroxene (Figure S3). The chromite within the plagioclase-chromite assemblage (on the basis of high-resolution, low-voltage EDS analysis) has Al_2O_3 in the range of 5.39–5.75 wt.%, which is a bit lower than the Al_2O_3 content of the chromite inside the shock melt vein (Al_2O_3 in the range of 6.41–6.66 wt.%). We found and characterized a total of five HP minerals in Slobodka, all located inside the major shock melt vein: albitic jadeite, tuite, majorite, wadsleyite, and xieite (Table S4), and analyzed in the following.

Albitic jadeite: The albitic jadeite occurs as submicron crystals within irregularly shaped felsic domains. Albitic jadeite structure was evaluated by EBSD, allowing us to confirm the *C*2/*c* clinopyroxene structure (Figure 4). The albitic jadeite has an empirical formula ($Na_{0.63–0.67}Ca_{0.07–0.08}K_{0.03–0.4}\square_{0.22–0.25}$)($Al_{0.85}Si_{0.13–0.15}Fe_{0.01–0.02}$)$Si_2O_6$ and Ca# [100 × Ca/ (Ca + Na)] in the range of 9.7–10.6, corresponding to a super-silicic clinopyroxene with 0.13–0.15 atoms per formula unit of octahedrally-coordinated Si. It approaches the nominal maximum of allowed

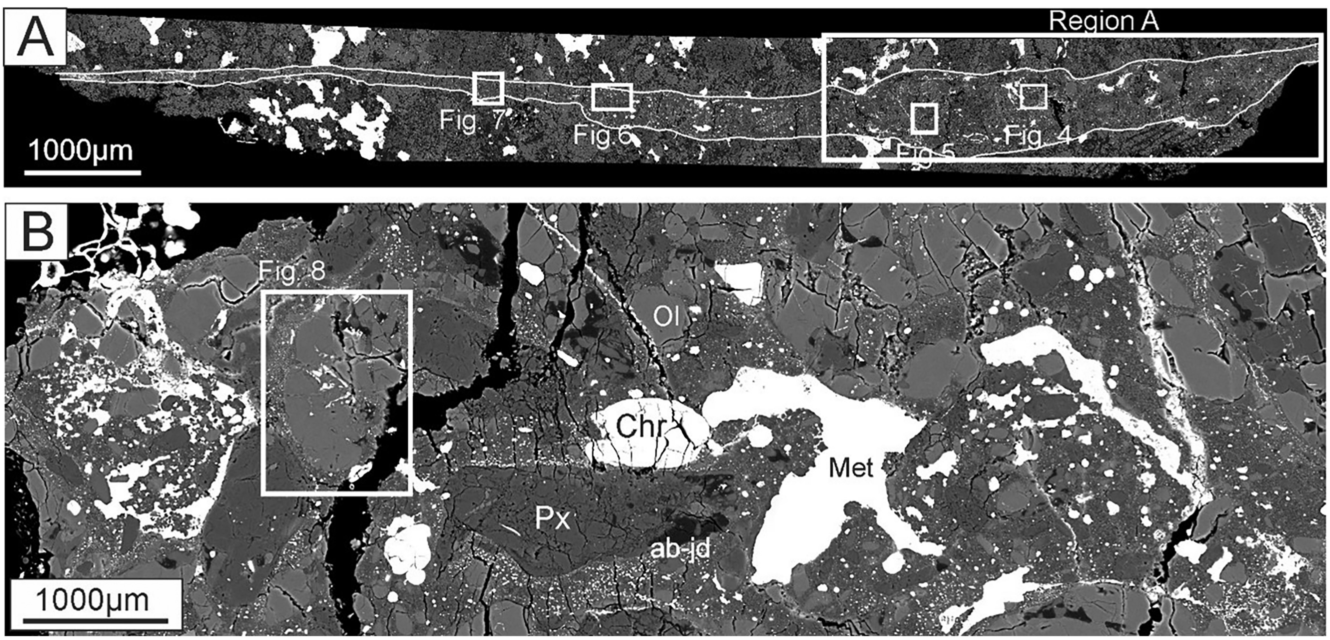

FIGURE 3 | (A) BSE mosaic showing an overview of the shock melt vein (MV) in the Slobodka NHMW-L4372 meteorite. Region A is denoted and further investigated with Raman spectroscopy (more details in figure 10). (B) Overview (back-scattered mosaic) of the investigated MV in the Slobodka NHMW-O2607 meteorite. The locations of the HP phases are denoted with white rectangles and further studied by means of Raman spectroscopy (Figures 5, 6, 7, 8, and 9).

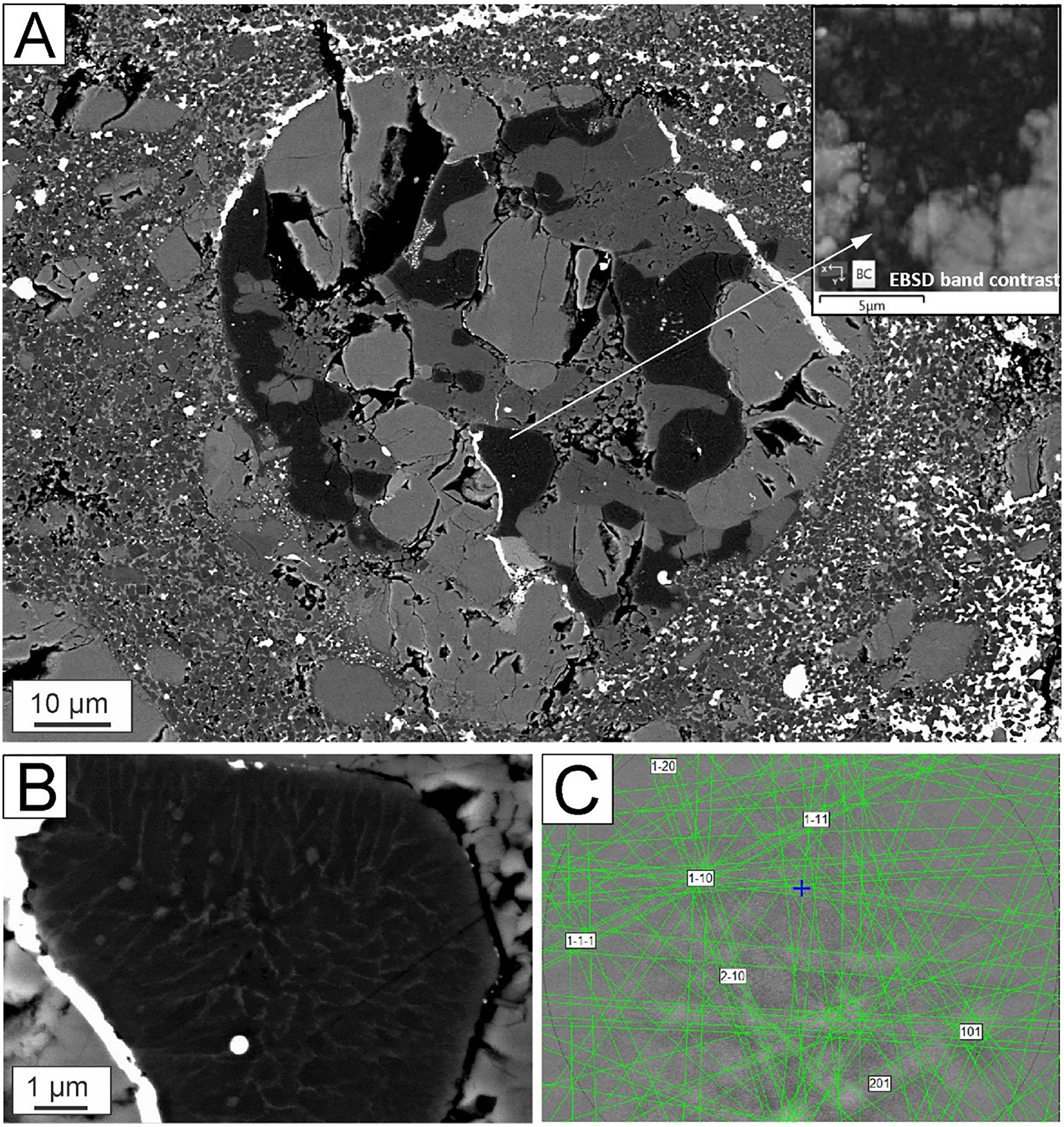

FIGURE 4 | (A) Composite clast embedded within MV hosting albitic jadeite; in the inset the EBSD band contrast. (B) Cellular texture of albitic jadeite. (C) EBSD pattern showing cpx structure only.

vacancies, up to ~0.25 per formula unit [2]. The albitic jadeite-bearing domains are up to ~32 μm long and are scattered all the way across the shock melt vein, from the center to the edges (Figure 5). We obtained close-up BSE images of various textures including cellular, acicular, as skeletal-hopper shapes [13, 14] (Figures 4, 5, and S4). BSE images acquired after conducting chemical analysis by EPMA show clear signs of beam damage. Some instances of albitic jadeite are beam-sensitive (e.g., in Chantonnay and Chug Chug 011 meteorites; [3]) and others are not (e.g., Ozerki meteorite; Baziotis et al. [2, 3, 5]; in this case, the evidence of beam-sensitivity led us to place our Raman spectroscopy spots in undamaged locations near but not precisely superimposed on EPMA spots.

It is noteworthy that the Raman spectrum of albitic jadeite is very similar to that of jadeite. Hence, Raman spectra alone are not adequate for discriminating jadeite from albitic jadeite [2–4]. The Raman spectra of albitic jadeite in Slobodka show major peaks at 700.5, 991, and 1040 cm^{-1} (Figure 5), matching the predominant peaks of the reference jadeite spectrum from the RRUFF database with peaks at ~700, 995, and 1045 cm^{-1}. Moreover, we have computed the theoretical Raman spectrum of albitic jadeite and confirmed that the difference from that of jadeite, while real, is too subtle to observe in most actual specimens [3]. To fully characterize the distribution of the albitic jadeite, we acquired Raman spectra for numerous points and estimated their distance from the center-line of the shock

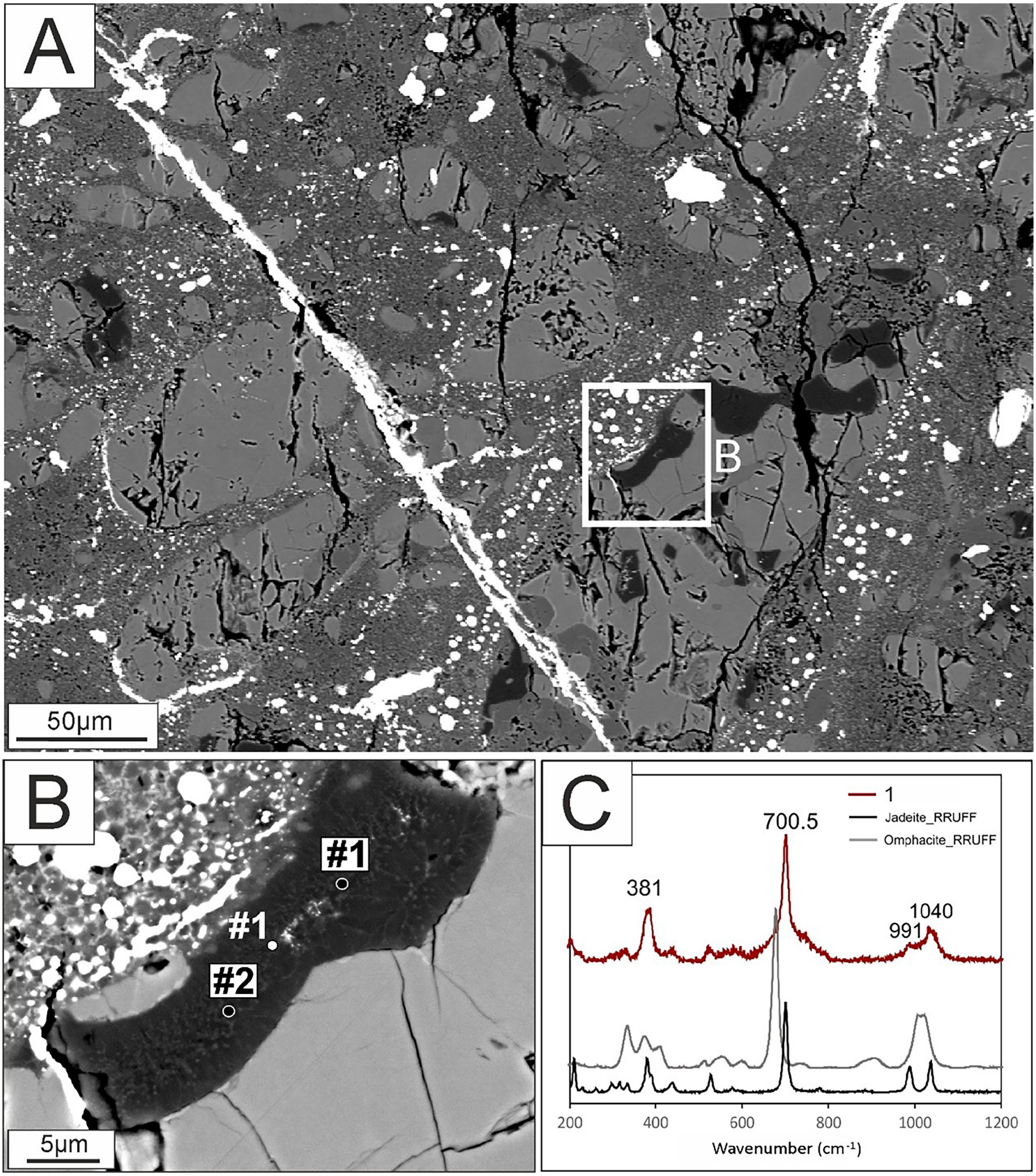

FIGURE 5 | (A) BSE image with selected position of analyzed albitic jadeite at the rim of a composite clast within the MV. (B) Locations of acquired Raman spectrum (white circle; #1) and EPMA analyses (black circles; #1 and #2) as given in Table S4. (C) Raman spectrum indicative of albitic jadeite (red line) from Slobodka section NHMW-L4372 compared to reference spectra from RRUFF database for jadeite (black line; RRUFF R050220.3) and for omphacite (gray line; RRUFF R061129). The Raman spectrum of albitic jadeite obtained using a 632.8 nm excitation wavelength.

melt vein. The Raman shift and full width at half maximum (FWHM) of the principal Raman peak of albitic jadeite near 700 cm^{-1} was calculated for each spectrum (Figure 10). We excluded spectra that did not have sufficient intensity able to define the major peak.

Tuite: The tuite is present as irregularly shaped crystals and as elongated crystals with a maximum length up to ~20 µm. It is scattered within the shock melt vein matrix (Figure 6). Its composition matches that of merrillite, with MgO content in the narrow range of ~3.62–3.67 wt.% and Na_2O of ~2.16–2.79 wt.% (Table S4).

The Raman spectrum of tuite exhibits a major peak at 978 cm^{-1}, lower intensity peaks at 410, 576, 1003 cm^{-1} and a broad minor peak at ~675 cm^{-1} (Figure 6). The spectrum matches the predominant peaks of the reference tuite in the RRUFF database (at ~977, 412, 577, and 1003 cm^{-1}), except for the broad peak, which may be due to nano-crystals of wüstite (which has peaks at 305 cm^{-1}, 529 cm^{-1}, and its strongest band at 662 cm^{-1} [15])

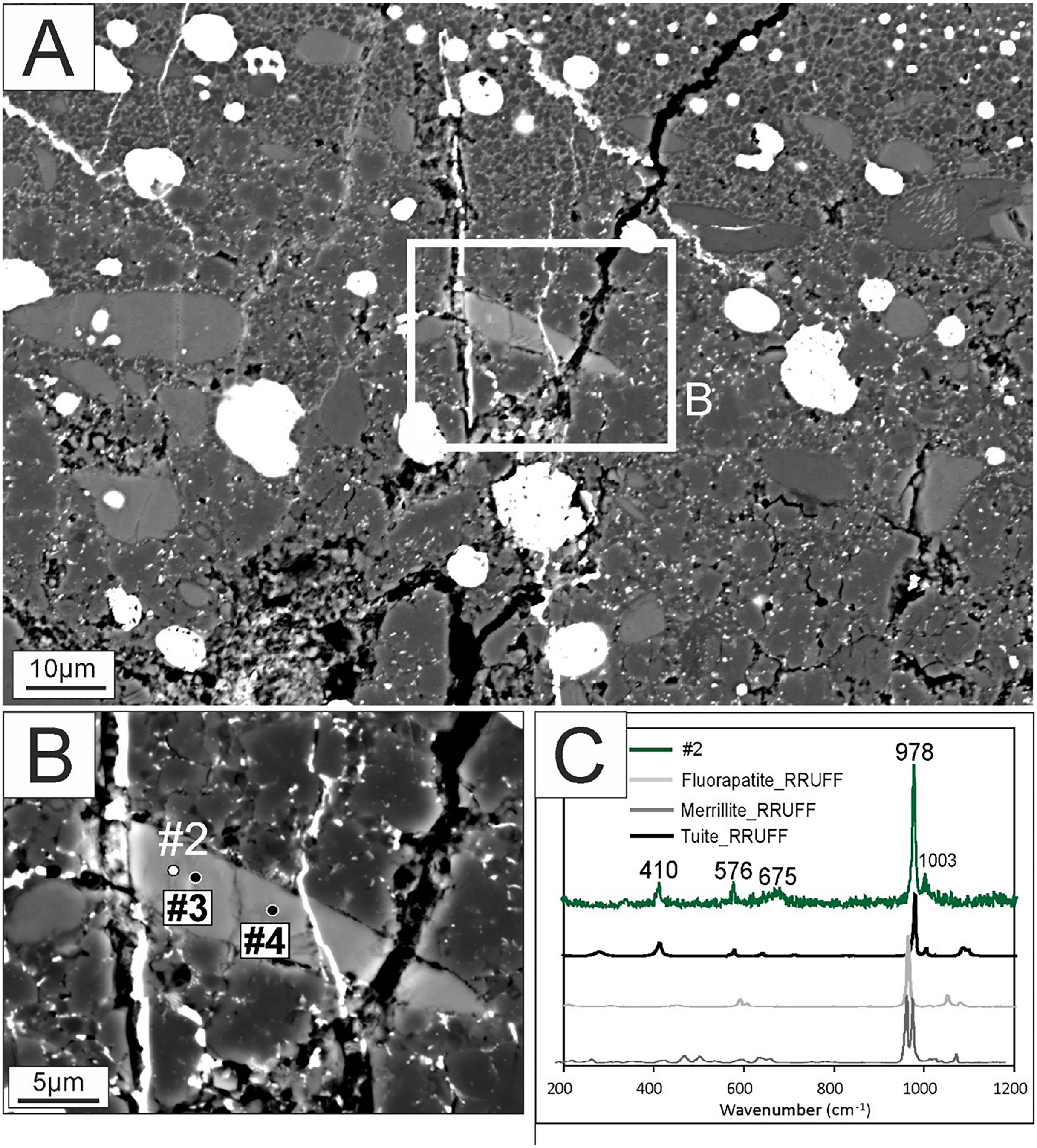

FIGURE 6 | (A) BSE image with selected position of analyzed tuite grain embedded in the groundmass of MV. (B) Locations of acquired Raman spectrum (white circle; #2) and EPMA analyses (black circles; #3 and #4) as given in Table S4. (C) Raman spectrum indicative of tuite (green line) from Slobodka section NHMW-L4372 compared to reference spectra from RRUFF database for tuite (black line; RRUFF R120115), for fluorapatite (light gray line; X050079) and merrillite (dark gray line; R150063). The Raman spectrum of albitic jadeite obtained using a 632.8 nm excitation wavelength.

somewhere within the excitation volume of the laser beam. The spectrum does not match that of fluorapatite or merrillite.

Majorite: Majorite garnet [16] is the most abundant mineral in the groundmass of the shock melt vein. It is present as blob-shaped clusters of small euhedral to subhedral crystals up to ~5–7 μm long (Figure 7). The majorite composition is in the range of $Ca_{0.18-0.20}Mg_{2.88-3.00}Fe_{0.54-0.57}Al_{0.01-0.36}Si_{3.81-3.90}O_{12}$ (Table S4). The Raman spectrum of majorite, with peaks at 670 and 929 cm^{-1} (Figure 7), matches the predominant peaks of the reference mineral in the RRUFF database, and is typical of meteoritic majorite occurrences (e.g., [3, 17]).

Wadsleyite: The wadsleyite forms lamellae ~6–8 μm wide in olivine crystals within the shock melt vein as well as narrow rims on olivine clasts (Figure 8); wadsleyite has a restricted compositional range, $Fa_{25.8-28.9}$ (Table S4). Raman analyses of the wadsleyite shows peaks at 718 and 917 cm^{-1} (Figure 8), matching the predominant peaks of the reference mineral in the RRUFF (720 and ~920 cm^{-1}).

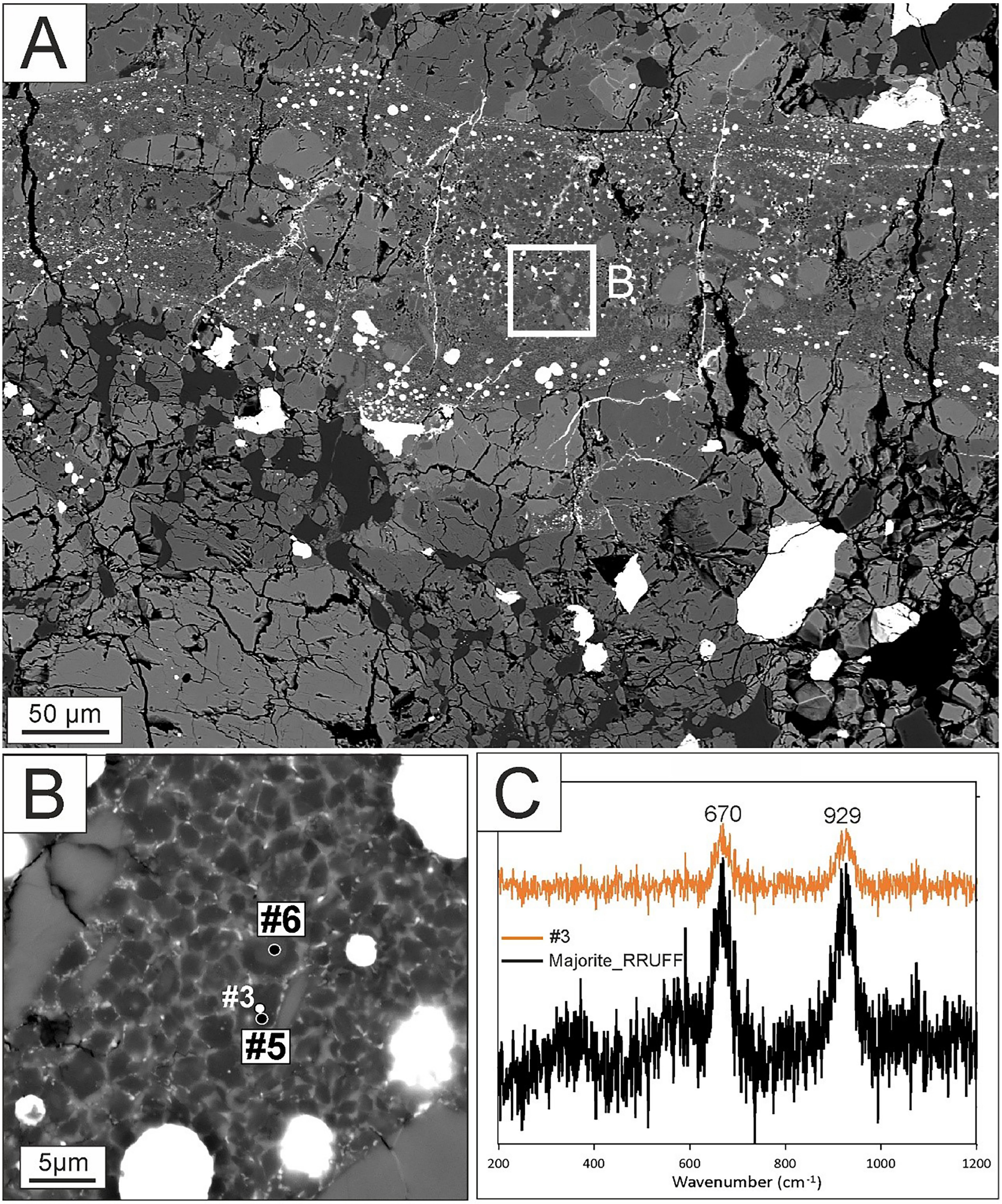

FIGURE 7 | (A) BSE image with selected position of analyzed majorite grain embedded in the groundmass of MV. (B) Locations of acquired Raman spectrum (white circle; #3) and EPMA analyses (black circles; #5 and #6) as given in Table S4. (C) Raman spectrum indicative of majorite (orange line) from Slobodka section NHMW-L4372 compared to reference spectrum from RRUFF database (black line; RRUFF R210005). The Raman spectrum of albitic jadeite obtained using a 514.5 nm excitation wavelength.

Xieite: The xieite appears in small chromite grains as polycrystalline aggregates [12, 18] (Figure 9). Xieite composition is in the range of $(Fe_{0.85-0.90}Mg_{0.17-0.30}Mn_{0.01-0.02})(Cr_{1.44-1.54}Al_{0.26-0.27}Ti_{0.06-0.07}V_{0.02})O_4$ (Table S4). The Raman spectrum acquired at spot #5 in Figure 9, with peaks at 605 and 685 cm^{-1}, matches the predominant peaks of the reference minerals in the RRUFF database for chromite (RRUFF R110059) and for xieite from Chen et al. [12]. The peak at ~685 cm^{-1} is typical of chromite and the ~605 cm^{-1} peak is specific to xieite [12].

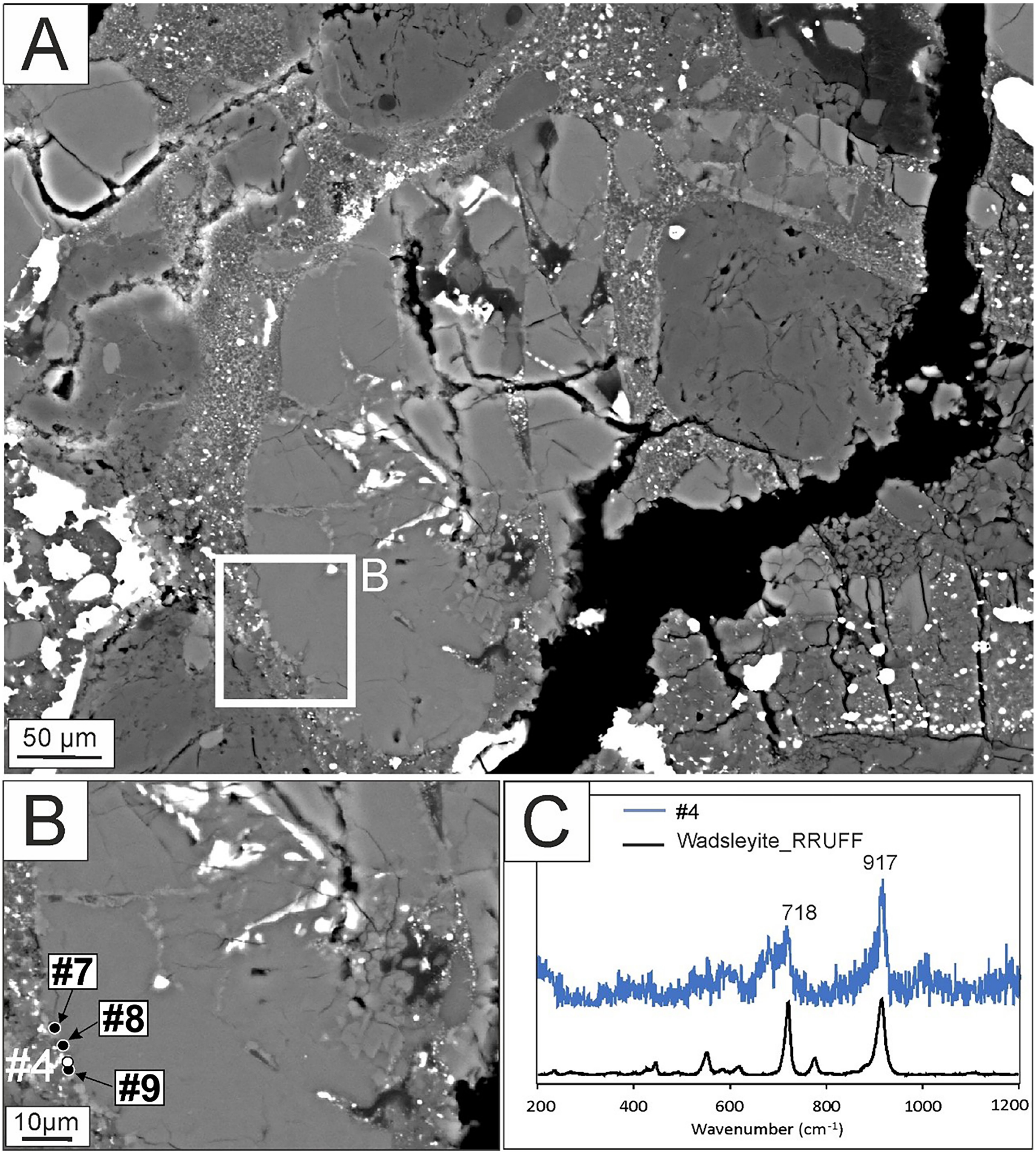

FIGURE 8 | (A) BSE image with selected position of analyzed wadsleyite grain at the rim of an olivine clast within the MV. (B) Locations of acquired Raman spectrum (white circle; #4) and EPMA analyses (black circles; #7, #8 and #9) as given in Table S4; it is important to note the wadsleyite lamellae over the olivine. (C) Raman spectrum indicative of wadsleyite (blue line) from Slobodka section NHMW-O2607 compared to reference spectrum of wadsleyite from RRUFF database (black line; RRUFF R090004, 532 nm). The Raman spectrum of albitic jadeite obtained using a 514.5 nm excitation wavelength.

4 | Discussion

4.1 | Classification of Slobodka Meteorite Revisited

We primarily base our evaluation of the classification of Slobodka on section NHMW-L4372, in which we evaluated in detail both the matrix and the shock melt vein (i.e., we focused exclusively on the shock melt vein area in section NHMW-O2607). The assignment to a chondrite group is based on several criteria including the mineral chemistry (silicates, metal, and sulfides), homogeneity of olivine compositions, structural state of low-Ca pyroxene, chondrule abundance, and metal abundance [19, 20]. Although the observed chondrule abundance in Slobodka is inconsistent with the typical 60–80% range expected for low petrologic types (3–4) in the H, L, and LL groups, it is typical for the recognizable chondrule fraction to be lower in the higher petrologic types (> 4)

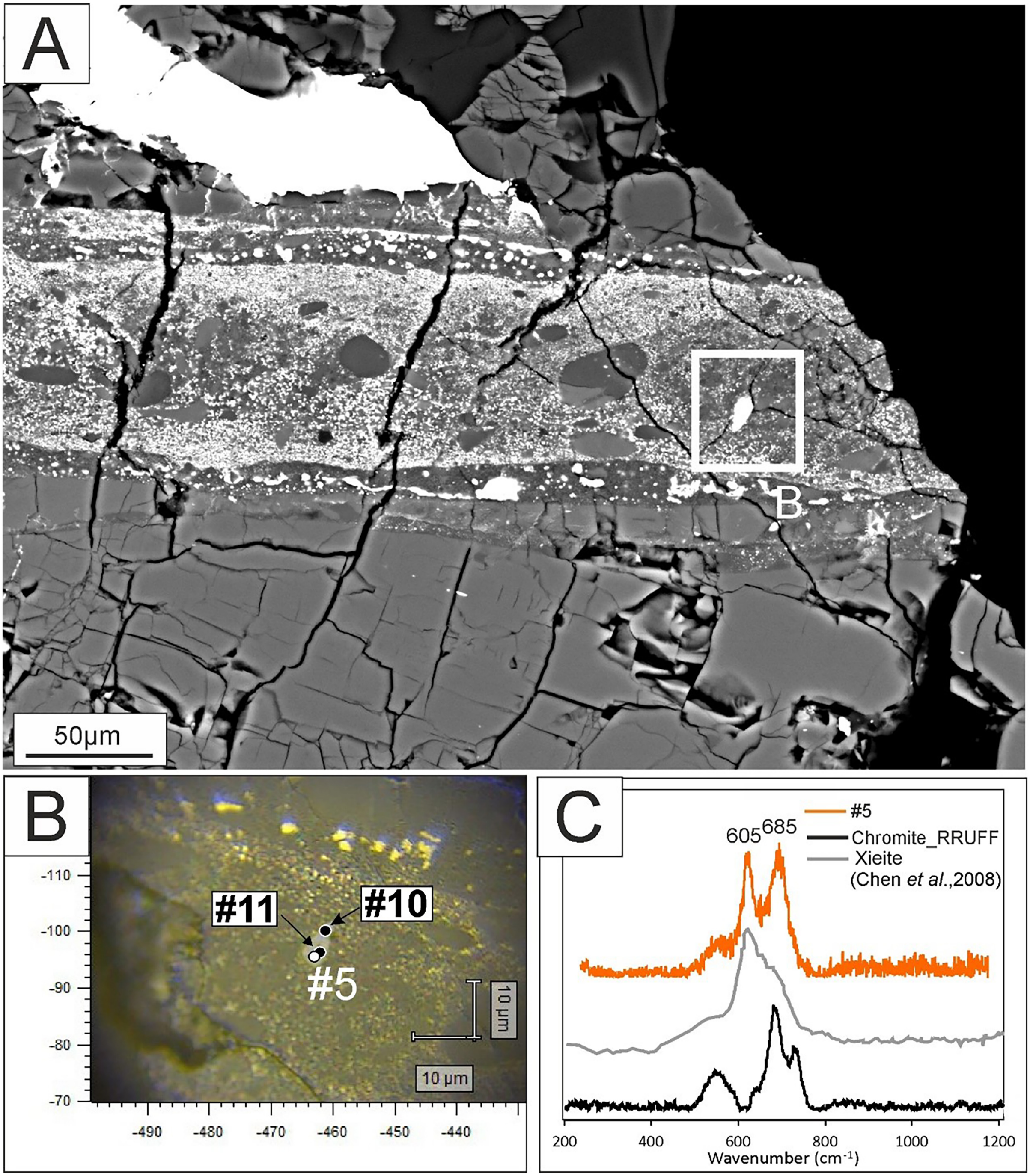

FIGURE 9 | (A) BSE image with selected position of analyzed xieite grain embedded in the groundmass of MV. (B) Locations of acquired Raman spectrum (white circle; #5) and EPMA analyses (black circles; #10 and #11) as given in Table S4. (C) Raman spectrum indicative of xieite (orange line) from Slobodka section NHMW-O2607 compared to reference spectrum of chromite from RRUFF database (black line; RRUFF R110059) and xieite from Chen et al. [12]. The Raman spectrum of albitic jadeite obtained using a 514.5 nm excitation wavelength.

in these groups [19]. The fayalite content of the olivine is in the range of 23–26 mol%, supporting assignment to the ordinary chondrite from the L group [19]. This is further suggested by the Fa histogram of figure S5. The metal abundance in the matrix is about 1.17 vol%, which is more typical of the LL group [19]. In contrast, the Co content in kamacite in Slobodka is in the range of 0.86–0.97 wt.% (Table S5). This is within the range suggested for L group by other researchers: 0.73–0.95 wt.% [21], 0.83–0.95 wt.% (Smith et al., 1993 [22]), and 0.67–0.82 wt.% [23]. The average Co values in kamacite for H and LL are respectively lower and higher than these L group values. Therefore, the Co content in kamacite of Slobodka is compatible with the L group. Considering the majority of the evidence, the most likely classification is L group [19, 20].

Regarding the petrologic type of Slobodka, we used the criteria described by Van Schmus and Wood [24]. In particular, the estimated maximum Ni contents in metal (29.85 wt.%) and in troilite (0.24 wt.%) suggest at least a type 3 [19]. The mean plagioclase grain size (~30 μm) implies that the plagioclase is metamorphic, which is most consistent with petrologic type 5. The blurring of chondrule boundaries is most consistent with type 4/5. Furthermore, the homogeneity test applied to olivine chemistry gives a mean standard deviation of 1.4%, which is consistent with type 4 [20]. However, it is important to note that Dodd's criterion offers weak discrimination among the more equilibrated chondrite types (L4 through L6). The Fe/Mn and Fe/Mg ratios of olivine and pyroxene crystals have been used for classifying the petrologic type of ordinary chondrites using the diagram of Gastineau-Lyons et al. [25]. For Slobodka, the Fe/Mn and Fe/Mg ratios (Figure S6) of olivine and clinopyroxene scatter across the L4, L5, and L6 fields and offer little insight. However, the orthopyroxene analyses consistently favor petrologic type L4. Considering all these criteria, L4 is the most likely petrologic type for the Slobodka meteorite.

Regarding the shock stage, most criteria are based on optical identification of shock microstructures (Table 1). The olivine exhibit weak mosaicism, low-grade planar fractures, planar deformation features, and undulatory extinction, while the low-Ca pyroxene exhibits undulatory extinction (Table 1). The plagioclase grains exhibit undulatory extinction and no maskelynite was found (Table 1). These features suggest a range of shock degree from weak (shock stage S2) to moderate (shock stage S4) [10]. Chromite has also been proposed as a shock indicator in ordinary chondrites. Furthermore, it is noteworthy that high-Al_2O_3 chromite-plagioclase clusters have been identified in the heavily-shocked Suizhou L6 ordinary chondrite meteorite [18]. As such, the chromite-plagioclase assemblages observed in Slobodka indicate at least shock stage S3 [27]. We refined the determination by mapping shock stage across the full thin section using the distribution of features described in Table 1 and the system of Stöffler et al. [10], in order to determine the area fraction, distribution, and contiguity of regions assigned to each shock stage (Figure S1B). Regions of shock stage S2 and S4 dominate the matrix; the S2 regions enclose a few small islands showing features characteristic of stage S3. The margins of the major shock melt vein are entirely bounded by regions of shock stage S4. Overall, we document significant heterogeneity of shock stage and therefore presumably of peak shock P and T at the single thin section scale (mesoscale); below we seek to quantify the significance of this pattern of shock stages in terms of peak shock conditions and the variability and distribution thereof.

4.2 | Pressure (P)–Temperature (T)–Time (T) Conditions

With a combination of crystallographic and compositional in situ analytical methods, we confirmed the presence of a number of high-pressure phases within the shock melt vein in Slobodka. These minerals include majorite, wadsleyite, tuite, xieite, and albitic jadeite. Here, we use these HP phases to constrain the shock and release path experienced by the shock melt vein.

Albitic jadeite has not been synthesized yet in any experiment and therefore its formation conditions are still poorly understood. In previously documented cases, its coexistence with other HP minerals with known stability ranges (e.g., majorite) has suggested its formation at 18–22 GPa [2]. More recently, however, Baziotis et al. [5], after a careful thermodynamic analysis, proposed 11.5 GPa as the most favorable pressure for albitic jadeite formation.

Tuite is likely formed from the transformation of merrillite and chlorapatite at a minimum P of 12 GPa at 1100 °C [28] but may require significantly higher P (20–23 GPa) at temperatures more appropriate to the liquidus of the shock melt vein (1900–2000 °C) [17, 29–31].

For majorite, which is a well-studied solid solution, we can use not only its presence but also its composition to constrain the pressure. The Collerson majorite barometer which is expressed by:

$$P\,(\mathrm{GPa}) = 5.78 + 18.23 \times X^{Cat}Mj, \quad (1)$$

where $X^{Cat}Mj$ represents the average value of two estimates of the majorite cation fraction, $X^{Cat}Mj_{(1)} = {}^{IV,VI}(\mathrm{Si}+\mathrm{Ti}) - 3 + {}^{VIII}\mathrm{Na}$ *and* $X^{Cat}Mj_{(2)} = [1-0.5\times{}^{VI}(\mathrm{Al}+\mathrm{Cr})] + {}^{VIII}\mathrm{M}^{2+}$ [32]. The texture of the MV hosting the majoritic garnet in Slobodka suggests crystallization from a liquid, indicated by the equigranular crystal shape and 120° triple junctions (Figure 7). Hence, the application of Collerson's barometer is valid, and yields a pressure range of 20.2–23.1 GPa. This is broadly consistent with the experimental data for tetragonal majorite, experimentally crystallized over a pressure range of 17–20 GPa at 1800 °C, and with P–T conditions inferred for majorite in other shocked meteorites [33–38].

In contrast, the inferred stability range of wadsleyite is widely accepted to occupy a lower pressure range of 14–18 GPa [39–41].

TABLE 1 | Observations on Slobodka meteorite (thin section NHMW-L4372) and assignment of shock stage of shock metamorphism for classification system C based on Stöffler et al. [10] (modified after [9, 26])

	SOX	UE	UE and PFs	WM and PFs	SM and PDFs	Phases in the melt zones	Shock stage
Olivine	–	+	+	+	–		S3-S4
Pyroxene	–	+	–	–	–		S2
Plagioclase	–	+	–	–	–		S2
Shock melt vein						LP, Ab-jd, Maj, Tui, Xie, Wds	S4

Abbreviations: +, the feature or features are present; –, the feature is absent; Ab-Jd, albitic jadeite; LP, low-pressure phases; Maj, majorite; PDFs, planar deformation features; PFs, planar fractures; SM, strong mosaicism; SOX, sharp optical extinction; Tui, tuite; UE, undulatory extinction; WM, weak mosaicism; Wds, wadsleyite; Xie, xieite.

Lastly, the xieite stability field extends from 20 to 23 GPa at 1800–1950 °C [42].

The coexistence of different HP phases in the same shock melt vein indicates a large heterogeneity, with recorded pressures spanning 12 to 23 GPa and temperatures between 1100 and 2100 °C. This suggests a temperature gradient during high-pressure mineral growth and a specific P–T–t path [7]. In particular, while pressure remained near its peak value (~23 GPa), the shock melt vein must have cooled below its liquidus enough to nucleate and grow several HP phases. We see evidence of growth from the melt of phases whose liquidus fields span a range of pressures. This implies that melt was present during a segment of the pressure–temperature–time path that included significant change in pressure. As there is no time for significant crystal nucleation and growth during the rise time of the shock (~1 ns), we conclude that the high-pressure phases are sampling a portion of the pressure release path after peak pressure. It follows that pressure release began before cooling of the melt vein crossed the solidus or the glass transition, such that pressure decrease occurred in the presence of melt from which phases could grow below the peak pressure. However, cooling must have been fast enough to prevent complete back-transformation to ambient-pressure minerals.

4.3 | Distribution of Albitic Jadeite Across the Shock Melt Vein

Utilizing our comprehensive Raman data, we sought to refine the effect of cooling rate on the character of recovered albitic jadeite by studying a transect across the main shock melt vein in Slobodka thin section NHMW-L4372 (Figure 10). The fit results reveal a positive correlation between the FWHM of the Raman 700 cm^{-1} peak and the relative distance from the center of the shock melt vein: albitic jadeite grains farther away from the center of the shock melt vein tend to exhibit higher FWHM values (Figure 11; Table S6). This trend is evident both above and below the center-line, as indicated by the linear fits with r^2 values of 0.73 and 0.72, respectively. The observed peak broadening with increasing relative distance from the center of the shock melt

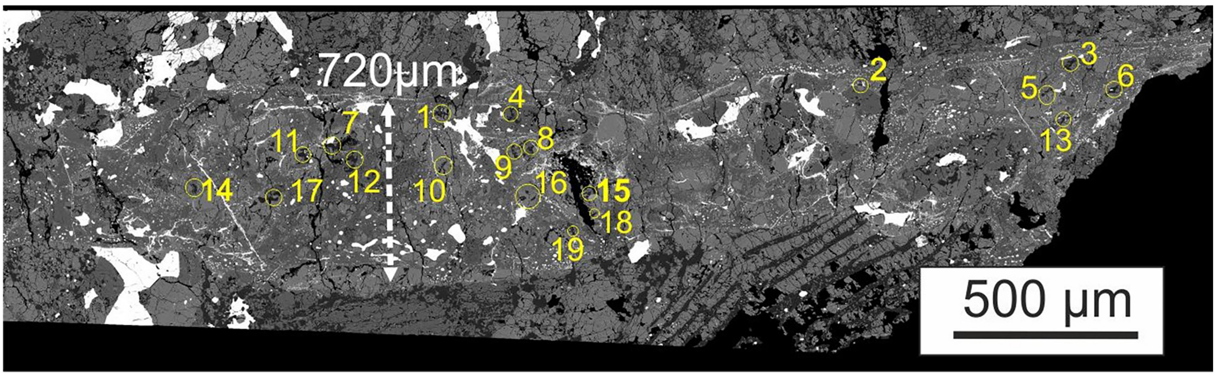

FIGURE 10 | BSE composite image with annotated regions of the albitic jadeite grains on region A within the MV.

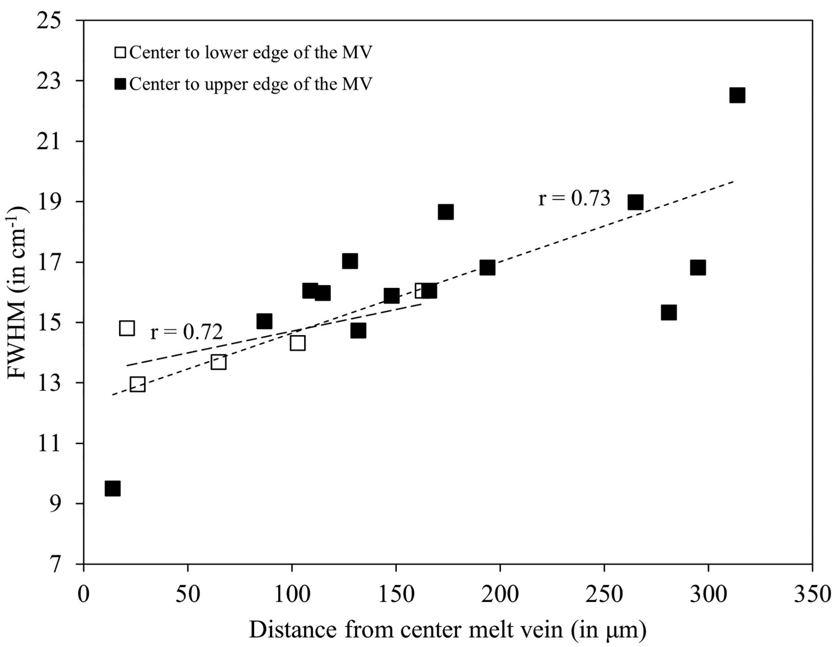

FIGURE 11 | FWHM results for the 700 cm^{-1} compared to the distance of the albitic jadeite from the center of the MV for the region A (Figure 10).

vein highlights structural and textural variations induced by shock metamorphism during the impact event.

The phenomenon of Raman peak broadening in albitic jadeite reported here has not been adequately studied for other HP phases. Experimental studies and meteorite observations both suggest Raman peak broadening with increasing shock level [43, 44], although the spatial distribution of shocked minerals in the melt was not extensively investigated. Such broadening should be attributable to crystallization dynamics that were, in turn, set by the spatially varying pressure–temperature–time path during albitic jadeite growth.

The formation of shock melt veins by shock compression is characterized by localized and transient high pressure and high temperature conditions. These conditions lead to melting and subsequent partial crystallization, including growth of high-pressure phases. It has been previously documented that the edges of shock melt veins experience faster cooling than their centers (e.g., in the L6 chondrite Château-Renard; [45]), because they cool by conduction to the surrounding matrix, which experienced a lower peak shock temperature. Thus, grains of HP phases located farther from the shock melt vein center likely experienced both higher thermal gradients and faster quenching rates, leading to residual stresses and lattice distortions. These stresses cause vibrational mode variations, resulting in broader Raman peaks. Additionally, structural disorder, such as microfractures, dislocations, point defects, and partial amorphization, may have developed near the edges, further contributing to peak broadening [43, 46]. In contrast, minerals located closer to the center of the shock melt vein are subjected to relatively prolonged thermal conditions, allowing for more complete crystallization and the formation of well-ordered structures, which are expected to exhibit sharper peaks in their Raman spectra like our observation.

Additionally, one theory for the development of localized shock melt veins in meteorites whose disseminated peak shock temperature does not approach the solidus is shear localization, leading to frictional or viscous heating and shear-induced melting. If that is the case, then there is another reason to expect a gradient in conditions across a shock melt vein, with shear stresses highest at the margins and lowest in the center (where viscosity is lowest). Crystal growth under shear stress modulates the crystallization process [47, 48], and growth under conditions of increasing shear stress with proximity to the shock melt vein margin is another potential mechanism for peak broadening as a systematic function of cross-vein position.

In summary, the systematic broadening of the main Raman peak in albitic jadeite as a function of proximity to the shock melt vein boundary that we discovered in Slobodka is a novel observation that calls for further investigations. It may be the result of one or more of several potential mechanisms: gradients in cooling rate, thermal gradient, and shear stress may all contribute to different crystallization dynamics and ultimately to variations in residual stress and structural disorder. Future investigations using techniques such as EBSD and Transmission Electron Microscopy will allow us to examine the microstructural characteristics of the albitic jadeite in greater details. These studies will offer additional insights into the mechanisms influencing the Raman spectra at various positions within the shock melt vein and help us refine our understanding of shock metamorphism and high-pressure phases formation in Slobodka and in shocked meteorites in general.

5 | Conclusions

Our investigation leads us to propose that the Slobodka meteorite is best classified as an L4 ordinary chondrite. Our determination of the meteorite's chondrite group and petrologic type is based on classification schemes that consider both textural (chondrule boundary visibility) and compositional data (olivine Fa 23–26 mol%; homogeneity of olivine analyses; Fe/Mn vs Fe/Mg for pyroxenes). The sample is variably shocked, with shock stages from S2 to S4, based on shock microstructures in olivine and pyroxene crystals (weak to moderate mosaicism; planar fractures, planar deformation features, undulatory extinction) and plagioclase (undulatory extinction; assemblage with chromite) and the presence of shock melt veins hosting high-pressure polymorphs. The shock melt vein contains five high-pressure polymorphs:albitic jadeite, tuite, majorite, xieite, and wadsleyite. The stability fields for these phases indicate pressures between 11.5 and 23 GPa and temperature variations spanning of 1100 to 2100 °C, with a complex but well-constrained path allowing growth and preservation of these phases. Cooling below the liquidus must have accompanied partial release of pressure to allow crystal growth at a range of pressures, while sufficient cooling must have been achieved before complete pressure release to stop back-transformation. We assessed the crystalline order of albitic jadeite as a function of position within the shock melt vein via the peak shape in its Raman spectrum; we proposed a range of mechanisms whereby proximity to the margin of the shock melt vein may have promoted greater structural disorder and broader peaks.

Acknowledgments

The authors are grateful to Wencke Wegner for assistance with the EPMA analyses. We are also grateful for the help from Michalis Sakalis for technical assistance during the SEM analyses at the Hellenic Survey of Geology & Mineral Exploration (HSGME) and the director of HSGME Demetrios Tarenidis for allowing MS to perform the analyses at no cost. We thank Alan Rubin and an anonymous reviewer for their constructive comments, which improved the original manuscript.

Conflicts of Interest

The authors declare no conflicts of interest.

Data Availability Statement

The data that supports the findings of this study are available in the supplementary material of this article

References

1. C. Hezel, K. A. Lehnert, P. Elangovan, P. Ji, J. Mays, and J. Koblitz, "The MetBase Database Has Been Merged Into Astromat," *Meteoritics & Planetary Science* 60 (2024): 143–148.

2. O. Ma, M. Tschauner, J. R. Kong, et al., "A High-Pressure, Clinopyroxene-Structured Polymorph of Albite in Highly Shocked

Terrestrial and Meteoritic Rocks," *American Mineralogist* 107, no. 4 (2022): 625–630.

3. S. Baziotis, A. Xydous, J. Papoutsa, et al., "Jadeite and Related Species in Shocked Meteorites: Limitations on Inference of Shock Conditions," *American Mineralogist: Journal of Earth and Planetary Materials* 107, no. 10 (2022): 1868–1877.

4. S. Baziotis, A. Xydous, J. Papoutsa, et al., "Investigation of the Shocked Viñales Ordinary Chondrite (L6) Meteorite Fall–Implications for Shock Classification, Fragmentation, and Collision Dynamics," *Icarus* 390 (2023): 115326.

5. C. Baziotis, S. Ma, J. Klemme, O. T. Berndt, and P. D. Asimow, "The High-Pressure, Vacancy-Stabilized Component in Clinopyroxenes," *American Mineralogist* (2025), https://doi.org/10.2138/am-2024-9609.

6. P. Rochette, L. Sagnotti, M. Bourot-Denise, et al., "Magnetic Classification of Stony Meteorites: 1. Ordinary Chondrites," *Meteoritics & Planetary Science* 38, no. 2 (2003): 251–268.

7. J. Hu and T. G. Sharp, "Formation, Preservation and Extinction of High-Pressure Minerals in Meteorites: Temperature Effects in Shock Metamorphism and Shock Classification," *Progress in Earth and Planetary Science* 9, no. 1 (2022): 1–22.

8. J. Fritz, A. Greshake, and V. A. Fernandes, "Revising the Shock Classification of Meteorites," *Meteoritics & Planetary Science* 52, no. 6 (2017): 1227–1232.

9. D. Stöffler and K. Keil, "Shock Metamorphism of Ordinary Chondrites," *Geochimica et Cosmochimica Acta* 55, no. 12 (1991): 3845–3867.

10. D. Stöffler, C. Hamann, and K. Metzler, "Shock Metamorphism of Planetary Silicate Rocks and Sediments: Proposal for an Updated Classification System," *Meteoritics & Planetary Science* 53, no. 1 (2018): 5–49.

11. N. Morimoto, "Die Nomenklatur von Pyroxenen," *Mineralogy and Petrology* 39 (1988): 55–76.

12. J. S. Chen and H. K. Mao, "Xieite, a New Mineral of High-Pressure $FeCr_2O_4$ Polymorph," *Chinese Science Bulletin* 53, no. 21 (2008): 3341–3345.

13. S. Ozawa, M. Miyahara, E. Ohtani, et al., "Jadeite in Chelyabinsk Meteorite and the Nature of an Impact Event on Its Parent Body," *Scientific Reports* 4 (2014): 5033.

14. M. J. Streck, "Mineral Textures and Zoning as Evidence for Open System Processes," *Reviews in Mineralogy and Geochemistry* 69, no. 1 (2008): 595–622.

15. E. Hazan, Y. Sadia, and Y. Gelbstein, "Characterization of AISI 4340 Corrosion Products Using Raman Spectroscopy," *Corrosion Science* 74 (2013): 414–418.

16. E. Ringwood and A. Major, "Synthesis of Majorite and Other High Pressure Garnets and Perovskites," *Earth and Planetary Science Letters* 12, no. 4 (1971): 411–418.

17. X. Xie, M. E. Minitti, M. Chen, et al., "Tuite, γ-$Ca_3(PO_4)_2$: A new Mineral From the Suizhou L6 Chondrite," *European Journal of Mineralogy* 15, no. 6 (2003): 1001–1005.

18. X. Xie, M. Chen, and C. Wang, "Occurrence and Mineral Chemistry of Chromite and Xieite in the Suizhou L6 Chondrite," *Science China Earth Sciences* 54 (2011): 998–1010.

19. M. K. Weisberg, T. J. McCoy, and A. N. Krot, "Systematics and Evaluation of Meteorite Classification," *Meteorites and the Early Solar System* II, no. 19 (2006): 19–52.

20. R. T. Dodd, Jr., W. R. Van Schmus, and D. M. Koffman, "A Survey of the Unequilibrated Ordinary Chondrites," *Geochimica et Cosmochimica Acta* 31, no. 6 (1967): 921–951.

21. E. Rubin, "Kamacite and Olivine in Ordinary Chondrites: Intergroup and Intragroup Relationships," *Geochimica et Cosmochimica Acta* 54, no. 5 (1990): 1217–1232.

22. G. Smith, Y. Miúra, and S. Launspach, "Fe, Ni and co Variations in the Metals of Some Antarctic Chondrites," *Earth and Planetary Science Letters* 120, no. 3–4 (1993): 487–498.

23. F. Afiattalab and J. T. Wasson, "Composition of the Metal Phases in Ordinary Chondrites: Implications Regarding Classification and Metamorphism," *Geochimica et Cosmochimica Acta* 44, no. 3 (1980): 431–446.

24. W. R. Van Schmus and J. A. Wood, "A Chemical-Petrologic Classification for the Chondritic Meteorites," *Geochimica et Cosmochimica Acta* 31, no. 5 (1967): 747–765.

25. H. K. Gastineau-Lyons, H. Y. McSween, Jr., and M. J. Gaffey, "A Critical Evaluation of Oxidation Versus Reduction During Metamorphism of L and LL Group Chondrites, and Implications for Asteroid Spectroscopy," *Meteoritics & Planetary Science* 37, no. 1 (2002): 75–89.

26. E. Rubin, E. R. Scott, and K. Keil, "Shock Metamorphism of Enstatite Chondrites," *Geochimica et Cosmochimica Acta* 61, no. 4 (1997): 847–858.

27. E. Rubin, "Chromite-Plagioclase Assemblages as a new Shock indicator; Implications for the Shock and Thermal Histories of Ordinary Chondrites," *Geochimica et Cosmochimica Acta* 67, no. 14 (2003): 2695–2709.

28. X. Xie, X. Gu, and M. Chen, "An Occurrence of Tuite, γ-$Ca_3(PO_4)_2$, Partly Transformed From ca-Phosphates in the Suizhou Meteorite," *Meteoritics & Planetary Science* 51 (2016): 195–202.

29. J. K. Murayama, S. Nakai, M. Kato, and M. Kumazawa, "A Dense Polymorph of Ca_3 $(PO_4)_2$: A High-Pressure Phase of Apatite Decomposition and Its Geochemical Significance," *Physics of the Earth and Planetary Interiors* 44 (1986): 293–303.

30. X. Xie, S. Zhai, M. Chen, and H. Yang, "Tuite, γ-$Ca_3(PO_4)_2$, Formed by Chloroapatite Decomposition in a Shock Vein of the Suizhou L6 Chondrite," *Meteoritics & Planetary Science* 48 (2013): 1515–1523.

31. S. Zhai, M. Akaogi, H. Kojitani, W. Xue, and E. Ito, "Thermodynamic Investigation on β- and γ-$Ca_3(PO_4)_2$ and the Phase Equilibria," *Physics of the Earth and Planetary Interiors* 228 (2014): 144–149.

32. K. D. Collerson, Q. Williams, B. S. Kamber, S. Omori, H. Arai, and E. Ohtani, "Majoritic Garnet: A new Approach to Pressure Estimation of Shock Events in Meteorites and the Encapsulation of sub-Lithospheric Inclusions in Diamond," *Geochimica et Cosmochimica Acta* 74, no. 20 (2010): 5939–5957.

33. N. Tomioka, M. Miyahara, and M. Ito, "Discovery of Natural $MgSiO_3$ Tetragonal Garnet in a Shocked Chondritic Meteorite," *Science Advances* 2 (2016): e1501725.

34. N. Tomioka and M. Miyahara, "High-Pressure Minerals in Shocked Meteorites," *Meteoritics & Planetary Science* 52 (2017): 2017–2039.

35. E. Ohtani, N. Kagawa, and K. Fujino, "Stability of Majorite (Mg,Fe) SiO_3 at High Pressures and 1800°C," *Earth and Planetary Science Letters* 102 (1991): 158–166.

36. T. Kato and M. Kumazawa, "Garnet Phase of $MgSiO_3$ Filling the Pyroxene–Ilmenite gap at Very High Temperature," *Nature* 316, no. 6031 (1985): 803–805.

37. S. Bazhan, K. D. Litasov, E. Ohtani, and S. Ozawa, "Majorite-Olivine–High-Ca Pyroxene Assemblage in the Shock-Melt Veins of Pervomaisky L6 Chondrite," *American Mineralogist* 102, no. 6 (2017): 1279–1286.

38. S. Heinemann, T. G. Sharp, F. Seifert, and D. C. Rubie, "The Cubic-Tetragonal Phase Transition in the System Majorite ($Mg_4Si_4O_{12}$)-pyrope ($Mg_3Al_2Si_3O_{12}$), and Garnet Symmetry in the Earth's Transition Zone," *Physics and Chemistry of Minerals* 24 (1997): 206–221.

39. Y. Fei and C. M. Bertka, "Phase Transitions in the Earth's Mantle and Mantle Mineralogy," *Mantle Petrology: Field Observations and High Pressure Experimentation* 6 (1999): 189–207.

40. T. Katsura and E. Ito, "The System Mg_2SiO_4-Fe_2SiO_4 at High Pressures and Temperatures: Precise Determination of Stabilities of Olivine, Modified Spinel, and Spinel," *Journal of Geophysical Research: Solid Earth* 94, no. B11 (1989): 15663–15670.

41. T. Katsura, H. Yamada, O. Nishikawa, et al., "Olivine-Wadsleyite Transition in the System $(Mg, Fe)_2SiO_4$," *Journal of Geophysical Research: Solid Earth* 109, no. B2 (2004): 1–12.

42. M. Chen, J. Shu, H. K. Mao, X. Xie, and R. J. Hemley, "Natural Occurrence and Synthesis of two new Postspinel Polymorphs of Chromite," *Proceedings of the National Academy of Sciences* 100, no. 25 (2003): 14651–14654.

43. S. Farrell-Turner, W. U. Reimold, M. Nieuwoudt, and R. M. Erasmus, "Raman Spectroscopy of Olivine in Dunite Experimentally Shocked to Pressures Between 5 and 59 GPa," *Meteoritics & Planetary Science* 40, no. 9–10 (2005): 1311–1327.

44. B. Zhang, S. R. Shieh, A. C. Withers, and A. Bouvier, "Raman Spectroscopy of Shocked Enstatite-Rich Meteorites," *Meteoritics & Planetary Science* 53, no. 10 (2018): 2067–2077.

45. P. D. Baziotis, J. Asimow, L. Hu, et al., "High Pressure Minerals in the Château-Renard (L6) Ordinary Chondrite: Implications for Collisions on Its Parent Body," *Scientific Reports* 8, no. 1 (2018): 9851.

46. A. Kereszturi, I. Gyollai, Z. Kereszty, et al., "Analyzing Raman–Infrared Spectral Correlation in the Recently Found Meteorite Csátalja," *Spectrochimica Acta Part a: Molecular and Biomolecular Spectroscopy* 173 (2017): 637–646.

47. F. Langenhorst, J. P. Poirier, A. Deutsch, and U. Hornemann, "Experimental Approach to Generate Shock Veins in Single Crystal Olivine by Shear Melting," *Meteoritics & Planetary Science* 37, no. 11 (2002): 1541–1553.

48. C. Hamann, K. Kurosawa, H. Ono, et al., "Experimental Evidence for Shear-Induced Melting and Generation of Stishovite in Granite at Low (< 18 GPa) Shock Pressure," *Journal of Geophysical Research: Planets* 128, no. 6 (2023): e2023JE007742.

Supporting Information

Additional supporting information can be found online in the Supporting Information section.